

Toward the unambiguous identification of supermassive binary black holes through Bayesian inference

XING-JIANG ZHU^{1,2} AND ERIC THRANE^{1,2}¹*School of Physics and Astronomy, Monash University, Clayton, VIC 3800, Australia*²*OzGrav: Australian Research Council Centre of Excellence for Gravitational Wave Discovery, Clayton, VIC 3800, Australia*

ABSTRACT

Supermassive binary black holes at sub-parsec orbital separations have yet to be discovered. In parallel with the global hunt for nanohertz gravitational waves from such binaries using pulsar timing arrays, there has been a growing sample of candidates reported from electromagnetic surveys, particularly searches for periodic variations in optical light curves of quasars. However, the periodicity search is prone to false positives from quasar red noise, especially when the data span is less than a few signal cycles. Here we present a Bayesian method for the detection of quasar periodicity in the presence of red noise. We apply this method to the binary candidate PG1302–102, using data from the Catalina Real-Time Transient Survey, the All-Sky Automated Survey for Supernovae (ASAS-SN) and the Lincoln Near-Earth Asteroid Research. We show that a) there is very strong support—with a Bayes factor greater than 10^5 —for periodicity, despite the fact that the inclusion of ASAS-SN data reduces the detection significance, and b) the prevalent damped random walk red-noise model is disfavored with more than 99% credibility. We discuss practical aspects of a periodicity search in time-series data and implications for the binary black hole nature of PG1302–102. Finally, we outline future work that may enable the unambiguous identification of supermassive binary black holes.

Keywords: supermassive black holes — quasars — galaxy mergers — Bayesian statistics

1. INTRODUCTION

Supermassive binary black holes are thought to be common in the Universe as natural products of galaxy mergers (Begelman et al. 1980). They are likely to be the primary sources of nanohertz gravitational waves, which have been actively searched for using pulsar timing arrays in the past decade (see, e.g., Hobbs et al. 2010; Verbiest et al. 2016; Perera et al. 2019, and references therein). Current pulsar timing arrays are sensitive to individual binaries, with component black hole masses $\gtrsim 10^9 M_\odot$ and binary orbital periods $\lesssim 10$ years (or orbital separations $\lesssim 0.01$ pc), up to distances of ~ 200 Mpc (Zhu et al. 2014; Babak et al. 2016; Aggarwal et al. 2019), though see Rosado et al. (2016) for the possibility of detecting high-redshift binaries. No detection has been made so far, although it has been suggested that the detection of a stochastic gravitational-wave background formed by the combined emission from binaries

across the Universe is likely in a few years (e.g., Taylor et al. 2016; Cordes & McLaughlin 2019).

The electromagnetic identification of sub-parsec supermassive binary black holes has proven to be challenging. Direct imaging of such close binaries is only possible for sources within ~ 100 Mpc via radio very-long-baseline interferometry observations. The closest binary with confident direct images, found in the radio galaxy 0402+379, has a separation of 7.3 pc (Rodriguez et al. 2006), corresponding to an orbital period of $\sim 10^4$ years (Bansal et al. 2017); See also Kharb et al. (2017) for a 0.35-pc binary candidate at 116 Mpc in the Seyfert galaxy NGC 7674. How binaries like these can reach milli-parsec orbital separations where the emission of gravitational waves can efficiently drive the binary to merge is referred to as the “final-parsec problem”, which remains an active area of theoretical investigations (e.g., Milosavljević & Merritt 2001; Yu 2002; Colpi 2014; Khan et al. 2016; Ryu et al. 2018; Goicovic et al. 2018; Muñoz et al. 2020). Finding a sub-parsec supermassive binary black hole would not only provide insights into the final-parsec problem, but also shed light on the expected stochastic gravitational-wave signal strength for pulsar timing arrays (Zhu et al. 2019; Goulding et al. 2019).

(Quasi-)periodically variable active galactic nuclei provide an interesting class of candidates for sub-parsec supermassive binary black holes. The most prominent object is OJ 287, a blazar which exhibits 12-year quasi-periodic outbursts in optical light curves that date back to the 19th century (Sillanpää et al. 1988; Valtonen et al. 2008). This periodicity has been interpreted by some authors as the secondary black hole crossing the accretion disk of the primary in an eccentric orbit (Valtonen et al. 2016; Dey et al. 2019). In the past five years, with the growth of time-domain astronomy, there have been a large number of sub-parsec supermassive binary black hole candidates claimed by various groups.

Based on the Catalina Real-time Transient Survey (CRTS), Graham et al. (2015a) put forward 111 binary black hole candidates from an optical variability analysis of 243,500 quasars. Among them, PG1302–102 was the most significant candidate with a measured period of 1884 days (Graham et al. 2015b). This periodicity has been attributed to the relativistic Doppler boosting of emission from a mini-disk around the secondary black hole (D’Orazio et al. 2015). Charisi et al. (2016) reported 33 binary candidates from a periodicity search in a sample of 35,383 quasars in the photometric database of the Palomar Transient Factory. Liu et al. (2015) identified a periodic variability of 542 days in quasar PSO J334.2+01.4 using data from the Pan-STARRS1 Medium Deep Survey. However, such a detection was found to be insignificant in a subsequent analysis of extended data (Liu et al. 2016); see Liu et al. (2019) for a systematic search over 9000 quasars which resulted in one candidate in their extensive analysis.

Following the periodicity report of PG1302–102, Vaughan et al. (2016) cautioned that the stochastic variability of normal quasars (i.e., those that do not host binary black holes) can easily resemble a periodic feature in light curves that span only a few periods and highlighted the importance of careful evaluation of false alarm rate. Through Bayesian model comparison, Vaughan et al. (2016) found a red noise model is significantly favoured against a pure sinusoidal model for PG1302–102. More recently, Liu et al. (2018) revisited the periodicity of PG1302–102 using additional data from the All-Sky Automated Survey for Supernovae (ASAS-SN). They employed a maximum likelihood method to search for a periodic signal in the presence of quasar red noise and found that the inclusion of ASAS-SN data reduced the periodicity significance. Therefore, Liu et al. (2018) concluded that the binary black hole model was disfavoured for PG1302–102. Kovačević et al. (2019) proposed a physical model that accounts for a cold spot in the accretion disk of the

primary black hole. Such a model can produce a perturbed sinusoidal feature and thus explain the apparent decrease in periodicity significance found by Liu et al. (2018).

Here, we propose a fully Bayesian framework for the identification of supermassive binary black hole candidates in time-domain electromagnetic surveys. It is capable of dealing with generic signal forms in the presence of red noise. Our work improves on previous studies in several ways. First, our method allows the inference of noise properties and signal parameters simultaneously and thus accounts for potential covariance between a periodic signal and quasar red noise. Second, it is robust to offsets in data collected with different surveys and possible over/under-estimation of measurement uncertainties. Third, we adopt a general form of quasar red noise and search for deviation from the commonly assumed damped random walk model (Kelly et al. 2009).

The remainder of this paper is organized as follows. In Section 2, we describe the Bayesian inference framework and introduce our signal and noise models. In Section 3, we apply the method to PG1302–102 with data from CRTS, ASAS-SN, and the Lincoln Near-Earth Asteroid Research (LINEAR) survey. In Section 4 we demonstrate practical aspects of a periodicity search through simulations. In Section 5 we discuss the implications of our analysis results for the binary black hole nature of PG1302–102. Last, we provide concluding remarks and outline directions for future work in Section 6.

2. BAYESIAN INFERENCE AND MODEL SELECTION OF TIME SERIES

In this section, we describe the framework of Bayesian inference and model selection for the analysis of time-series data. We focus on the case of searching for periodicity in quasar light curves—quasar brightness measurements as a function of time. Assuming stationary Gaussian noise, the likelihood function for a quasar light curve is

$$\mathcal{L}(\mathbf{d}|\vec{\theta}_n, \vec{\theta}_s, m) = \frac{1}{\sqrt{(2\pi)^N |\mathbf{C}|}} \exp \left[-\frac{1}{2} (\mathbf{d} - \mathbf{m} - \mathbf{s})^T \mathbf{C}^{-1} (\mathbf{d} - \mathbf{m} - \mathbf{s}) \right], \quad (1)$$

where \mathbf{d} is the time-series light curve data with length N . In this work we use measurements of optical magnitudes (i.e., the logarithmic light curve). The data \mathbf{d} is modeled as

$$\mathbf{d} = \mathbf{n} + \mathbf{m} + \mathbf{s}, \quad (2)$$

where \mathbf{n} is the noise vector, which contains measurement uncertainties and additional intrinsic stochastic quasar variability; \mathbf{m} is a constant vector with identical entries

of m , and m accounts for the mean magnitude and any constant offset (e.g., constant level of contamination due to host galaxy light); the signal vector \mathbf{s} is given by

$$\mathbf{s}(t) = A \sin(2\pi f_0 t + \phi). \quad (3)$$

The signal parameters are $\vec{\theta}_s = \{A, \phi, f_0\}$, where the signal frequency f_0 is related to the orbital period: $f_0 = 1/T_0$. In Equation (1), $\mathbf{C}_{ij} = \langle \mathbf{n}_i \mathbf{n}_j \rangle$ is the noise covariance matrix, which contains two components, $\mathbf{C} = \mathbf{C}_w + \mathbf{C}_r$, where \mathbf{C}_w is a diagonal matrix that represents measurement uncertainties, and \mathbf{C}_r accounts for the stochastic quasar variability, usually termed “red noise.”

In the damped random walk model (Kelly et al. 2009), the power spectral density of stochastic quasar variabilities takes the following form

$$P(f) = \frac{2\hat{\sigma}^2\tau_0^2}{1 + (2\pi\tau_0 f)^2}, \quad (4)$$

where $\hat{\sigma}^2$ is the intrinsic variance between observations on short timescales (~ 1 day), and τ_0 is the damping timescale. The noise covariance matrix is

$$\mathbf{C}_{ij} = (\nu\sigma_i)^2\delta_{ij} + \frac{1}{2}\hat{\sigma}^2\tau_0 \exp\left(-\frac{\tau_{ij}}{\tau_0}\right), \quad (5)$$

where σ_i is the measurement uncertainty for the i th observation, ν is a scale factor used to quantify the over/under-estimation of measurement uncertainties, δ_{ij} is the Kronecker delta function, and $\tau_{ij} \equiv |t_i - t_j|$. The noise parameters are $\vec{\theta}_n = \{\hat{\sigma}, \tau_0, \nu\}$.

To account for the possibility that the quasar red noise deviates from the damped random walk model (e.g., Zu et al. 2013; Guo et al. 2017), we also consider the following form of noise covariance matrix:

$$\mathbf{C}_{ij} = (\nu\sigma_i)^2\delta_{ij} + \frac{1}{2}\hat{\sigma}^2\tau_0 \exp\left[-\left(\frac{\tau_{ij}}{\tau_0}\right)^\gamma\right]. \quad (6)$$

The second part is the stretched exponential function¹. Note that the special case of $\gamma = 1$ corresponds to the damped random walk model, $\gamma = 0$ means white noise, and $\gamma = 2$ reduces to the Gaussian function. We illustrate the red-noise models in Appendix A.

We use Bayesian model selection to quantify the statistical significance of the presence of periodic signals in quasar light curves. We start with Bayes’ theorem, which states that

$$P(\vec{\theta}|\mathbf{d}, \mathcal{H}) = \frac{\mathcal{L}(\mathbf{d}|\vec{\theta}, \mathcal{H})P(\vec{\theta}|\mathcal{H})}{\mathcal{Z}(\mathbf{d}|\mathcal{H})}. \quad (7)$$

¹ In the context of describing relaxation in disordered systems, it is called the Kohlrausch-Williams-Watts function.

Here $P(\vec{\theta}|\mathbf{d}, \mathcal{H})$ is the posterior probability distribution function of parameters $\vec{\theta}$ given data \mathbf{d} and hypothesis \mathcal{H} ; $\mathcal{L}(\mathbf{d}|\vec{\theta}, \mathcal{H})$ is the likelihood function given in Equation (1), which describes the probability of observing data given the hypothesis \mathcal{H} and parameters $\vec{\theta}$. Meanwhile, $P(\vec{\theta}|\mathcal{H})$ is the prior distribution of parameters $\vec{\theta}$ while $\mathcal{Z}(\mathbf{d}|\mathcal{H})$ is the Bayesian evidence for hypothesis \mathcal{H}

$$\mathcal{Z}(\mathbf{d}|\mathcal{H}) = \int d\vec{\theta} \mathcal{L}(\mathbf{d}|\vec{\theta}, \mathcal{H})P(\vec{\theta}|\mathcal{H}). \quad (8)$$

Given the observational data, we wish to compare two hypotheses: \mathcal{H}_n = the data are consistent with only noise (i.e., $\mathbf{s} = 0$), and \mathcal{H}_s = there is a periodic signal present in the data. The ratio of posterior probability, called the *odds ratio*, between hypotheses \mathcal{H}_s and \mathcal{H}_n is:

$$\mathcal{O} = \frac{P(\mathcal{H}_s|\mathbf{d})}{P(\mathcal{H}_n|\mathbf{d})} = \frac{\mathcal{Z}(\mathbf{d}|\mathcal{H}_s)P(\mathcal{H}_s)}{\mathcal{Z}(\mathbf{d}|\mathcal{H}_n)P(\mathcal{H}_n)}, \quad (9)$$

where $P(\mathcal{H}_n)$ and $P(\mathcal{H}_s)$ are the prior probability for hypotheses \mathcal{H}_n and \mathcal{H}_s , respectively. Assuming equal prior probability for both hypotheses, Bayesian model selection is usually performed by computing the Bayes factor:

$$\mathcal{B}_n^s = \frac{\mathcal{Z}(\mathbf{d}|\mathcal{H}_s)}{\mathcal{Z}(\mathbf{d}|\mathcal{H}_n)}. \quad (10)$$

In this work, we are primarily concerned with the support for a periodic signal quantified by \mathcal{B}_n^s . We also wish to compute the support for deviation from the damped random walk model, by comparing two models involving Equations (6) and (5). Following Kass & Raftery (1995), the interpretation of Bayes factors is as follows. In a natural logarithmic scale, $0 < \ln \mathcal{B} < 1$ indicates that the support (for the hypothesis in the numerator) “worth no more than a bare mention,” $1 < \ln \mathcal{B} < 3$ implies positive support, $3 < \ln \mathcal{B} < 5$ implies strong support and $\ln \mathcal{B} > 5$ implies very strong support. These thresholds are somewhat arbitrary; $\ln \mathcal{B} = 8$ is often adopted as the detection threshold in gravitational-wave astronomy (e.g., Thrane & Talbot 2019).

3. APPLICATION TO PG1302–102

PG1302–102 is a nearby bright quasar with a median V-band magnitude of 15.0 at a redshift of $z = 0.2784$. We apply our method to light-curve data—V-band magnitude measurements—collected with CRTS (Drake et al. 2009), ASAS-SN (Shappee et al. 2014; Jayasinghe et al. 2019), and LINEAR (Sesar et al. 2011). The CRTS data are publicly available² as part of the Catalina Surveys Data Release 2, including 290 photometric measurements taken between 6 May 2005 and 30 May 2013.

² <http://nesssi.cacr.caltech.edu/DataRelease/>

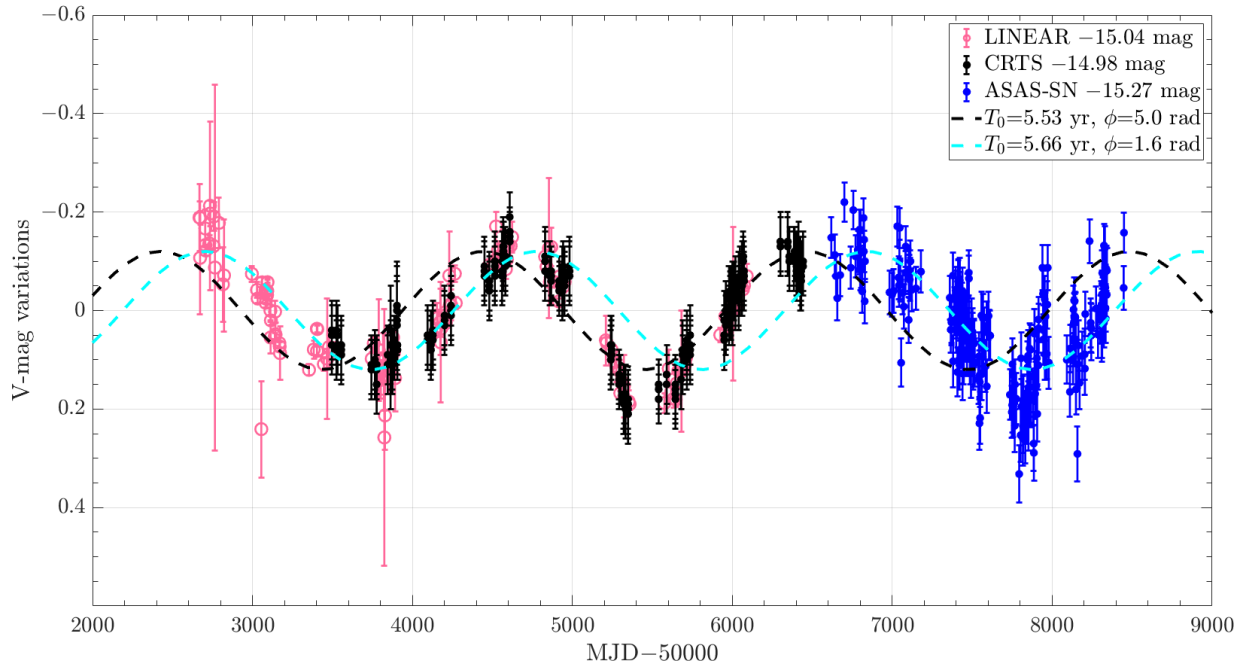


Figure 1. The light curve of PG1302–102 from LINEAR (pink), CRTS (black) and ASAS-SN (blue). Mean magnitudes have been subtracted, and the LINEAR data shown here are averaged from original measurements with an interval of 1 day. The two dashed sinusoidal curves (in black and cyan colors) represent example fits to the data.

The ASAS-SN data are downloaded from its photometry database³ as part of their Data Release 9, including 232 measurements acquired between 23 November 2013 and 27 November 2018. The LINEAR data contain 626 measurements made between 23 January 2003 and 12 June 2012. The median measurement uncertainties are 0.06, 0.05 and 0.01 mag for CRTS, ASAS-SN and LINEAR data, respectively. The span of the combined data set is 15.84 years. To reduce the computational cost, we average LINEAR data with an interval of 1 day, which reduces the number of points to 138. The bin size is chosen such that any stochastic time-correlated variations over a timescale greater than 1 day are preserved. The new uncertainty for binned data is computed as the standard deviation of original measurements inside the binning window. The median uncertainty for averaged LINEAR data is 0.015 mag. Figure 1 shows the data used in our analysis. Also shown are two sinusoidal curves representing possible fits to the data.

To implement the analysis outlined in Section 2 using PG1302–102 data, we employ the *Bilby* software package (Ashton et al. 2019), which is a general and versatile Bayesian inference library developed primarily for gravitational-wave astronomy. For the stochastic sampling of posteriors and evidence calculation, we use

the dynamic nested sampling method developed by Higgs et al. (2019), which is available through the *Dynesty* package (Speagle 2020).

Our priors are specified in Table 1. The log-normal priors for the damped random walk model parameters $\hat{\sigma}^2$ and τ_0 are the same as those used in Vaughan et al. (2016), which were based on earlier studies of quasar red noise under the damped random walk model (MacLeod et al. 2010; Kozłowski et al. 2010; Andrae et al. 2013). For the remaining parameters, we assign uniform priors. There is one mean magnitude m and one white-noise scaling factor ν for each data set (CRTS, ASAS-SN and LINEAR), leading to a total of 12 parameters for the combined data.

Parameter	Prior description
A (mag)	Uniform, min=0, max=0.5
ϕ (radian)	Uniform, min=0, max= 2π
T_0 (yr)	Uniform, min=0, max=10
m (mag)	Uniform, min=14.5, max=15.5
ν	Uniform, min=0.1, max=2
$\ln \hat{\sigma}^2$ ($\text{mag}^2 \text{ yr}^{-1}$)	Normal, mean=-4.0, width=1.15
$\ln \tau_0$ (yr)	Normal, mean=-0.6, width=1.15
γ	Uniform, min=0, max=2

Table 1. Priors used in the analysis.

³ <https://asas-sn.osu.edu/photometry>

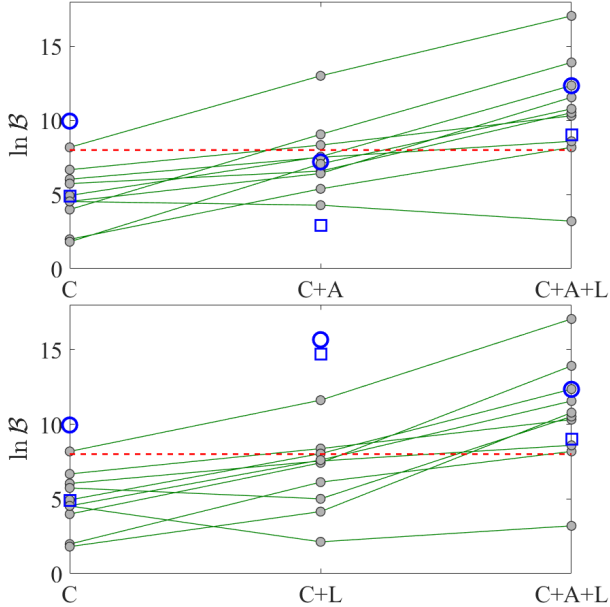


Figure 2. The natural logarithm of Bayes factor ($\ln \mathcal{B}$) for different combinations of data sets: C – CRTS, A – ASAS-SN, L – LINEAR. Blue symbols are for real data, whereas grey filled circles are for simulated data; all results compare the sinusoidal signal hypothesis against the noise hypothesis, except blue squares which indicate the level of support for deviation from the damped random walk model. The red dashed horizontal line marks $\ln \mathcal{B} = 8$.

3.1. Results

Using CRTS data alone, we find that the damped random walk (i.e., no sinusoidal signal) model is overwhelmingly favoured over the sinusoidal model (i.e., no red noise), with $\ln \mathcal{B} = 180$ ($\log_{10} \mathcal{B} = 78$). This matches with the result of $\log_{10} \mathcal{B} > 60$ computed in [Vaughan et al. \(2016\)](#). However, it may be argued that the choice between pure red noise and pure sinusoid is a false dilemma as we expect a realistic signal to be characterized by both red noise *and* a sinusoidal signal. The question investigated here therefore is whether or not there is a sinusoidal signal *on top of* red noise. The corresponding physical picture is that fluctuations in the accretion disk of the primary black hole (or the circumbinary disk) produces red noise and the binary motion results in periodic variations.

In Figure 2, blue open circles show the log Bayes factor comparing the sinusoidal+general red noise hypothesis (Eq. 6) to the red-noise-only hypothesis for different combinations of data sets. There is strong support for the sinusoidal signal across all cases and the strongest support ($\ln \mathcal{B} = 15.7$) arises from the CRTS and LINEAR combination. One can see that the significance decreases considerably, with a reduction of log Bayes

factor around 3, when the ASAS-SN data set is added. This is consistent with the finding of [Liu et al. \(2018\)](#), which interpreted it as evidence against the periodicity. (We present our own interpretation in the next two subsections.) Using all available data, the sinusoidal-signal hypothesis is favoured with a log Bayes factor of 12.3 ($\mathcal{B} = 2.2 \times 10^5$) against the red-noise-only hypothesis.

Blue squares in Figure 2 compare the general red noise (Eq. 6) model to the damped random walk (Eq. 5) model: $\gamma \in [0, 2]$ v.s. $\gamma = 1$. There is a similar trend in the reduction of Bayes factor when ASAS-SN data is added. Using all three data sets, we find that the damped random walk model is significantly disfavoured, with a Bayes factor of 8000 ($\ln \mathcal{B} = 9$). In Appendix B, we present the full posterior distributions for two hypotheses—red noise only (Figure 5) and sinusoidal signal plus red noise (Figure 6)—when all data are used. We present key take-away messages here.

First, all parameters are well-constrained with Gaussian-like 1-D marginalized posterior distributions, except the signal period T_0 and phase ϕ . The distribution of (T_0, ϕ) is bimodal. We attribute this feature to the covariance between red noise and the periodic model—a significantly longer data span is required to precisely measure parameters than what is required to claim a detection. The two posterior modes are $T_0 = 5.53$ yr (2020 days), $\phi = 5.0$ rad, and $T_0 = 5.66$ yr (2067 days), $\phi = 1.6$ rad. We plot in Figure 1 the sinusoidal signal associated with each mode, setting $A = 0.12$ mag (the median posterior probability amplitude) in both cases. These two curves provide a sense of the $1-\sigma$ uncertainty in the sinusoidal variations.

Second, as indicated by the Bayes factors (plotted as blue squares in Figure 2), there is conclusive support for deviation from a damped random walk model. As shown in Figure 6, the exponential index γ is measured to be $0.62^{+0.06}_{-0.06}$, ruling out $\gamma = 1$ with more than 99% credibility. The red-noise time scale τ_0 is around 1 yr. In the red-noise-only hypothesis, the posteriors of (γ, τ_0) shift toward larger $\gamma \approx 0.77$ and longer τ_0 (~ 3 yr). This is expected given that the signal period is greater than the red-noise time scale. Such a feature demonstrates the covariance between periodic signal and red noise, and the importance to measure both properties simultaneously.

Third, estimates of the constant offset (or equivalently the mean magnitude) m and white-noise scaling factor ν are consistent between Figures 5 and 6. This is unsurprising because these parameters are uncorrelated with the periodic signal term. We find the magnitude measurement uncertainties of CRTS are significantly overestimated by a factor of 5 ($\nu = 0.21^{+0.01}_{-0.01}$), whereas those of ASAS-SN are slightly underestimated by 15%

($\nu = 1.15^{+0.06}_{-0.05}$). For LINEAR, we find $\nu = 0.96^{+0.12}_{-0.14}$, which is consistent with 1. This is expected because the error bars are estimated as the standard deviation of original measurements inside a 1-day averaging window. Applying our method to the original LINEAR data⁴ results in $\nu = 2.91^{+0.09}_{-0.10}$, implying the LINEAR measurement uncertainties are significantly underestimated.

4. PRACTICAL ASPECTS OF A PERIODICITY SEARCH

4.1. *What does it mean that the significance of the periodicity in PG1302-102 goes down when we add more data?*

The growth in periodicity significance is not guaranteed in the presence of red noise. A red-noise process produces long-term correlations in the data, meaning the noise component in new data is not independent from old data. To demonstrate this effect, we inject a periodic signal into 10 random realizations of quasar red noise. We choose exactly the same sampling and error bars as shown in Figure 1. Each of the 10 data sets contain three subsets, from LINEAR, CRTS and ASAS-SN. We compute the Bayes factor (comparing the sinusoidal signal plus red noise model against the red-noise-only model) for different combinations of subsets.

We choose the following parameters, motivated by posterior estimates of PG1302-102 shown in Figure 6: $A = 0.12$ mag, $T_0 = 5.53$ yr, $\phi = 5.0$ rad, $\ln \hat{\sigma}^2 = -2.56$ mag² yr⁻¹, $\ln \tau_0 = 0.15$ yr, $\gamma = 0.62$, $\nu_{\text{CRTS}} = 0.21$, $\nu_{\text{LINEAR}} = 0.96$ and $\nu_{\text{ASAS-SN}} = 1.15$. The red noise realization is generated using $\mathbf{n} = \mathbf{L}\mathbf{r}$. Here \mathbf{L} is a lower triangular matrix obtained from the Cholesky decomposition of the noise covariance matrix $\mathbf{C} = \mathbf{L}\mathbf{L}^T$ where \mathbf{L}^T is the conjugate transpose of \mathbf{L} . The $N \times 1$ vector of \mathbf{r} contains N independent random numbers that follow the standard normal distribution.

We plot the Bayes factors from 10 simulated light curves of PG1302-102 in Figure 2 as grey filled circles with lines. Several features are noteworthy. First, the general trend is that Bayes factors grow when we add LINEAR and ASAS-SN data to CRTS data. Second, there are two noise realizations where the addition of LINEAR data onto CRTS data results in a reduced detection significance of periodicity; in one of these two realizations, the addition of ASAS-SN data also lead to a reduced Bayes factor. We note that these two realizations have relatively low initial Bayes factors ($\ln \mathcal{B} \lesssim 6$). Therefore, we conclude that 1) whether or not the periodicity significance grows with the inclusion of a certain

set of additional data cannot be used as a simple criterion for true periodicity; 2) the periodicity significance is highly likely to grow with time once it is already in a signal-dominated regime. A rule of thumb for when does this occur is a threshold of log Bayes factor of 8.

This simulation study highlights the challenge in the periodicity search in quasar light curves; namely, there is only one realisation of the red noise. This situation is in contrast with the search for continuous gravitational waves (also essentially sinusoidal signals) using pulsar timing arrays. Many millisecond pulsars in the timing array have been found to exhibit red noise for which the origin is largely unknown. However, these red noise processes, if intrinsic to pulsars themselves, are not expected to correlate among different pulsars. A false detection caused by red noise in one particular pulsar can be ruled out by cross-checking other pulsar data. In order to overcome the challenge in establishing a supermassive binary black detection through periodicity searches, it is necessary to search for other signatures, including gravitational waves.

4.2. *How does binning affect the detection significance and parameter estimation?*

It is common that some sort of averaging or binning is applied when analysing time-series data. Information is inevitably lost in this process. Here we demonstrate the potentially adverse effect of binning on the periodicity detection significance and parameter estimation precision with an example. We choose the data set that gives rise to the highest log Bayes factor in the previous subsection. Because the LINEAR data used in this work have already gone through an averaging process with an interval of 1 day, we only use simulated data for CRTS and ASAS-SN. Figure 3 shows the simulated data, their binned versions with an interval of 100 days, and the injected periodic signal.

We compute two Bayes factors: a) a sinusoidal signal plus general red noise hypothesis against the red-noise-only hypothesis, and b) a sinusoidal signal plus general red noise hypothesis against a sinusoidal signal plus the damped random walk red noise hypothesis. Cases a) and b) indicate the level of support for periodicity and for deviation from damped random walk model, respectively. The log Bayes factors are 13.0 and 6.3 for case a) and b), respectively, using the original data. These Bayes factors become 7.7 and -0.1 for case a) and b), respectively, using the binned data. Therefore, the binning process not only reduces our ability to detect a periodicity but also to identify deviation from the damped random walk red-noise model.

⁴ The prior on ν is uniform on the interval $[0.5, 5]$.

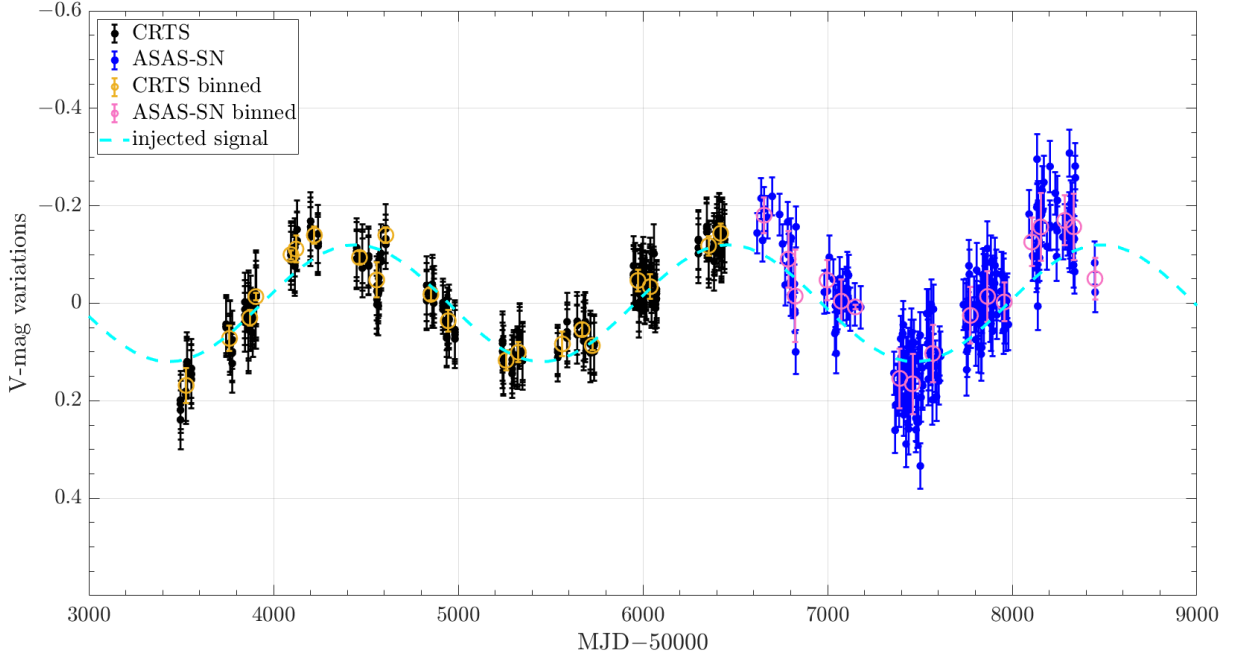


Figure 3. A simulated light curve of PG1302-102 that includes an injected sinusoidal signal. Mean magnitudes have been subtracted. Filled circles are original data, whereas open circles are binned data with an interval of 100 days.

Posterior distributions for this injection study are shown in Appendix C in Figures 7 (unbinned data) and 8 (binned data). The binning process generally broadens the posterior distributions of both signal and noise parameters; we discuss this in greater detail in Section 6. Note, in particular, that γ posteriors for binned data are uninformative, which agrees with the Bayes factor ($\ln \mathcal{B} = 0$) that shows the two red-noise models are indistinguishable. A similar multimodal feature in the 2-D posterior of $T_0 - \phi$ can be seen in both Figures 6 and 7. This can be attributed to the fact that we are estimating red noise and the periodic signal parameters simultaneously, and the data cover only a few (~ 3) signal cycles.

4.3. On the implementation of our method to a large sample of quasar light curves

The computational cost in our analysis is dominated by the computation of the inverse and determinant of the $N \times N$ noise covariance matrix associated with the likelihood evaluation, which scales as N^3 . For the entire data set of PG1302-102 analysed in this work, $N = 660$. A single likelihood evaluation takes on the order of 0.1 seconds and the full parameter estimation and evidence calculation for such a data set take about 48 hours on a single modern CPU core. The computational cost is the reason why we choose to average LINEAR data in an interval of 1 day, which reduce the total number of data points from 1148 to 660. Furthermore, there are a large number of quasars for which

long-term photometric measurements are available, for example 10^5 quasars from the CRTS as processed in [Graham et al. \(2015a\)](#). Therefore, further speed-up of our method is highly desirable.

This is a well-known problem in the analysis of astronomical time series. In pulsar timing arrays, there are normally hundreds to thousands of times of arrival measurements for each pulsar and the problem involves correlation analysis with data from dozens of pulsars. Various acceleration/approximation techniques have been proposed to enable full Bayesian analysis of pulsar timing array data. One popular method is to approximate the red noise as the sum of k Fourier components, and thus its covariance matrix is given by $\mathbf{C} = \mathbf{F}\mathbf{\Phi}\mathbf{F}^T$ where \mathbf{F} is $N \times k$ (with $k \ll N$) and $\mathbf{\Phi}$ is a $k \times k$ diagonal matrix. This turns the computationally heavy inversion of \mathbf{C} into the lower-rank diagonal matrix inversion $\mathbf{\Phi}^{-1}$ through the Woodbury matrix lemma (e.g., [van Haasteren & Valisneri 2015](#); [Lentati et al. 2013](#)). Elsewhere, [Foreman-Mackey et al. \(2017\)](#) proposed a fast Gaussian-process model that makes use of the feature where the covariance function can be expressed as a mixture of complex exponentials. Implemented as the `celerite` package, its computational cost scales linearly with the size of the data set. Both of these methods may prove useful for the analysis of light curves for a large number of quasars within the Bayesian framework developed here.

5. ON THE BINARY BLACK HOLE NATURE OF PG1302–102

Our analysis show that the combined CRTS+ASAS-SN+LINEAR data set favours the presence of a periodicity of $5.53 - 5.66$ years (68% credibility) with $\ln \mathcal{B} = 12.34$, which is lower than the $\ln \mathcal{B} = 15.66$ for the CRTS+LINEAR data. In either case, the Bayes factor indicates undeniable evidence for periodicity—the signal hypothesis is at least $\sim 10^5$ times more probable than the noise hypothesis. However, PG1302–102 was selected as the most significant candidate from $\sim 10^5$ quasars, which means a trials factor of 10^5 needs to be included in the calculation of false alarm probability. To properly account for the trials factor in Bayesian analysis is non-trivial⁵, and we leave it to a future work where we apply our method to a large sample of quasars.

The inclusion of ASAS-SN data not only reduce the Bayes factors in favour of a periodicity or deviation from damped random walk red noise (see Figure 2), but also significantly shifts the posterior distributions of both signal and noise parameters. With the CRTS+LINEAR data, we obtain $T_0 = 5.21^{+0.14}_{-0.16}$ yr, $\ln \hat{\sigma}^2 = -3.1^{+0.14}_{-0.08} \text{ mag}^2 \text{ yr}^{-1}$, $\ln \tau_0 = 0.75^{+0.38}_{-0.13}$ yr, and $\gamma = 0.48^{+0.05}_{-0.05}$. This is contrasted to $T_0 = 5.56^{+0.10}_{-0.03}$ yr, $\ln \hat{\sigma}^2 = -2.56^{+0.12}_{-0.14} \text{ mag}^2 \text{ yr}^{-1}$, $\ln \tau_0 = 0.15^{+0.36}_{-0.39}$ yr, and $\gamma = 0.62^{+0.06}_{-0.06}$ after adding ASAS-SN data. The two sets of distributions are inconsistent at $> 2\text{-}\sigma$ level. In fact, if we analyse the ASAS-SN data alone, we find negligible support for a periodicity ($\ln \mathcal{B} = 1.2$) or deviation from the damped random walk red-noise model ($\ln \mathcal{B} = 1.5$).

This comparison is an example of what is known as a posterior predictive check, in which one performs sanity tests to make sure the models are suitable for Bayesian inference. The instability of posterior distributions with the inclusion of more data may suggest our signal+noise model does not fully describe the data: either the signal is not a pure sinusoid, or the red noise is more complicated than Equation (6), or both. For the former case, the model proposed by Kovačević et al. (2019), which invokes a cold spot in the accretion disk of the primary black hole, might be an interesting alternative for model selection.

6. CONCLUSIONS

⁵ The frequentist false alarm probability is a quantity based on a particular noise model. However, as we conclude later on, our work indicates that the current “periodic signal plus red noise” model for PG1302–102 is probably incomplete. Therefore, the false alarm probability, even properly calculated, is likely not a useful metric in this case.

Sub-parsec supermassive binary black holes are crucial in our understanding of galaxy evolution. They are also the primary sources of nanohertz gravitational waves highly anticipated by international pulsar timing array campaigns. While nearly impossible to resolve through direct imaging, such close binaries are expected to produce periodic variations in light curves of active galactic nuclei. New candidates of periodicity are reported on a nearly monthly basis.

In this work, we propose a fully Bayesian method for the identification of periodicity in astronomical time-series that exhibit red noise. We apply this method to one of the most promising periodicity candidates, PG1302–102, using data from CRTS, ASAS-SN and LINEAR surveys. Our main findings are:

1. The CRTS and LINEAR data strongly favour the presence of a periodicity with $\ln \mathcal{B} = 16$. There is also conclusive evidence for deviation from the damped random walk red-noise model, with $\ln \mathcal{B} = 15$.
2. The ASAS-SN data are inconsistent with CRTS and LINEAR observations, as they provide no support for a periodicity or deviation from the damped random walk model. Their inclusion in the analysis reduces the statistical support ($\ln \mathcal{B}$ decreases by ≈ 3) for both features, and gives rise to posterior distributions that are inconsistent at $> 2\text{-}\sigma$ level. We interpret this to mean that our signal+noise model is incomplete.

We further perform simulations and demonstrate the following:

1. For data sets like LINEAR, CRTS and ASAS-SN, it is possible to obtain reduced periodicity significance with the inclusion of additional data because of the stochastic fluctuations of red noise. However, this is unlikely to happen in the signal-dominated regime ($\ln \mathcal{B} \gtrsim 8$).
2. Given the strong periodicity in CRTS or LINEAR data ($\ln \mathcal{B} \approx 10$), the reduction in $\ln \mathcal{B}$ associated with ASAS-SN indicates the incompleteness of our sinusoidal+red noise model.
3. The use of data binning can reduce our ability to detect periodicity or deviation from the damped random walk model, because the binning throws away high-frequency information that is helpful for estimating the spectral slope of the red noise (see Figure 4).

While we are unable here to settle the “binary or not” question for PG1302–102, our analysis shows that it is

an interesting object that warrants continuing efforts in observations and theoretical modelling. Our Bayesian framework can be adopted to establish unambiguous binary black hole detections with the following extensions:

1. Apply this method to various physical models for the periodicity, such as periodic mass accretion rate of the binary (e.g., [Farris et al. 2014](#)) or jet precession of a single or binary supermassive black holes (e.g., [Abraham & Carrara 1998](#); [Kudryavtseva et al. 2011](#); [Britzen et al. 2018](#)), in addition to relativistic Doppler boosting;
2. Use more sophisticated signal models that account for a cold-spot-induced perturbation in the accretion disk for PG1302–102 ([Kovačević et al. 2019](#)) or post-Newtonian orbital evolution for OJ 287 ([Dey et al. 2018](#));
3. Combine multi-wavelength observations (e.g., [Xin et al. 2019](#)), and other signatures associated with a binary black hole, for example, Doppler velocity offsets in broad emission line profiles ([Eracleous et al. 2012](#); [Bon et al. 2012](#); [Li et al. 2016](#)), flux deficits in the spectral energy distribution ([Gültekin & Miller 2012](#); [Yan et al. 2015](#); [Guo et al.](#)

[2020](#)), and kinematic signatures in reverberation-mapping data of active galactic nuclei ([Wang et al. 2018](#)). See [Zheng et al. \(2016\)](#) for a binary black hole candidate for which different types of signatures are analyzed;

4. Use astrophysically-motivated population priors. For example, the period distribution of binary black hole population is expected to be dominated by long periods, and the distribution of red-noise parameters can be obtained by applying our method to a large number of active galactic nuclei using hierarchical inference. We discuss practical ways to speed up our analysis to make the latter feasible.

We thank Tingting Liu for sharing the PG1302–102 data used in [Liu et al. \(2018\)](#). We thank Boris Goncharov and Yuri Levin for useful discussions. This work is supported by ARC CE170100004 and ARC FT150100281. The Catalina Sky Survey is funded by NASA under Grant No. NNG05GF22G issued through the Science Mission Directorate Near-Earth Objects Observations Program. The CRTS survey is supported by the U.S. National Science Foundation under grants AST-0909182 and AST-1313422.

REFERENCES

- Abraham, Z., & Carrara, E. A. 1998, *ApJ*, 496, 172
- Aggarwal, K., et al. 2019, *ApJ*, 880, 116
- Andrae, R., Kim, D. W., & Bailer-Jones, C. A. L. 2013, *A&A*, 554, A137
- Ashton, G., Hübner, M., Lasky, P. D., et al. 2019, *ApJS*, 241, 27
- Babak, S., Petiteau, A., Sesana, A., et al. 2016, *MNRAS*, 455, 1665
- Bansal, K., Taylor, G. B., Peck, A. B., Zavala, R. T., & Romani, R. W. 2017, *ApJ*, 843, 14
- Begelman, M. C., Blandford, R. D., & Rees, M. J. 1980, *Nature*, 287, 307
- Bon, E., Jovanović, P., Marziani, P., et al. 2012, *ApJ*, 759, 118
- Britzen, S., Fendt, C., Witzel, G., et al. 2018, *MNRAS*, 478, 3199
- Charisi, M., Bartos, I., Haiman, Z., et al. 2016, *MNRAS*, 463, 2145
- Colpi, M. 2014, *SSRv*, 183, 189
- Cordes, J., & McLaughlin, M. A. 2019, *BAAS*, 51, 447
- Dey, L., Valtonen, M. J., Gopakumar, A., et al. 2018, *ApJ*, 866, 11
- Dey, L., Gopakumar, A., Valtonen, M., et al. 2019, *Universe*, 5, 108
- D’Orazio, D. J., Haiman, Z., & Schiminovich, D. 2015, *Nature*, 525, 351
- Drake, A. J., Djorgovski, S. G., Mahabal, A., et al. 2009, *ApJ*, 696, 870
- Eracleous, M., Boroson, T. A., Halpern, J. P., & Liu, J. 2012, *ApJS*, 201, 23
- Farris, B. D., Duffell, P., MacFadyen, A. I., & Haiman, Z. 2014, *ApJ*, 783, 134
- Foreman-Mackey, D., Agol, E., Ambikasaran, S., & Angus, R. 2017, *AJ*, 154, 220
- Goicovic, F. G., Maureira-Fredes, C., Sesana, A., Amaro-Seoane, P., & Cuadra, J. 2018, *MNRAS*, 479, 3438
- Goulding, A. D., Pardo, K., Greene, J. E., et al. 2019, *ApJL*, 879, L21
- Graham, M. J., Djorgovski, S. G., Stern, D., et al. 2015a, *MNRAS*, 453, 1562
- . 2015b, *Nature*, 518, 74
- Gültekin, K., & Miller, J. M. 2012, *ApJ*, 761, 90

- Guo, H., Liu, X., Tayyaba, Z., & Liao, W.-T. 2020, *MNRAS*, 492, 2910
- Guo, H., Wang, J., Cai, Z., & Sun, M. 2017, *ApJ*, 847, 132
- Higson, E., Handley, W., Hobson, M., & Lasenby, A. 2019, *Statistics and Computing*, 29, 891
- Hobbs, G., et al. 2010, *Class. Quant. Grav.*, 27, 084013
- Jayasinghe, T., Stanek, K. Z., Kochanek, C. S., et al. 2019, *MNRAS*, 485, 961
- Kass, R. E., & Raftery, A. E. 1995, *Journal of the American Statistical Association*, 90, 773
- Kelly, B. C., Bechtold, J., & Siemiginowska, A. 2009, *ApJ*, 698, 895
- Khan, F. M., Fiacconi, D., Mayer, L., Berczik, P., & Just, A. 2016, *ApJ*, 828, 73
- Kharb, P., Lal, D. V., & Merritt, D. 2017, *Nature Astronomy*, 1, 727
- Kovačević, A. B., Popović, L. Č., Simić, S., & Ilić, D. 2019, *ApJ*, 871, 32
- Kozłowski, S., Kochanek, C. S., Udalski, A., et al. 2010, *ApJ*, 708, 927
- Kudryavtseva, N. A., Britzen, S., Witzel, A., et al. 2011, *A&A*, 526, A51
- Lentati, L., Alexander, P., Hobson, M. P., et al. 2013, *PhRvD*, 87, 104021
- Li, Y.-R., Wang, J.-M., Ho, L. C., et al. 2016, *ApJ*, 822, 4
- Liu, T., Gezari, S., & Miller, M. C. 2018, *ApJL*, 859, L12
- Liu, T., Gezari, S., Heinis, S., et al. 2015, *ApJL*, 803, L16
- Liu, T., Gezari, S., Burgett, W., et al. 2016, *ApJ*, 833, 6
- Liu, T., Gezari, S., Ayers, M., et al. 2019, *ApJ*, 884, 36
- MacLeod, C. L., Ivezić, Ž., Kochanek, C. S., et al. 2010, *ApJ*, 721, 1014
- Milosavljević, M., & Merritt, D. 2001, *ApJ*, 563, 34
- Muñoz, D. J., Lai, D., Kratter, K., & Mirand a, R. 2020, *ApJ*, 889, 114
- Perera, B. B. P., et al. 2019, *MNRAS*, 490, 4666
- Rodriguez, C., Taylor, G. B., Zavala, R. T., et al. 2006, *ApJ*, 646, 49
- Rosado, P. A., Lasky, P. D., Thrane, E., et al. 2016, *PhRvL*, 116, 101102
- Ryu, T., Perna, R., Haiman, Z., Ostriker, J. P., & Stone, N. C. 2018, *MNRAS*, 473, 3410
- Sesar, B., Stuart, J. S., Ivezić, Ž., et al. 2011, *AJ*, 142, 190
- Shappee, B. J., Prieto, J. L., Grupe, D., et al. 2014, *ApJ*, 788, 48
- Sillanpää, A., Haarala, S., Valtonen, M. J., Sundelius, B., & Byrd, G. G. 1988, *ApJ*, 325, 628
- Speagle, J. S. 2020, *MNRAS*, 493, 3132
- Taylor, S. R., Vallisneri, M., Ellis, J. A., et al. 2016, *ApJL*, 819, L6
- Thrane, E., & Talbot, C. 2019, *PASA*, 36, e010
- Valtonen, M. J., et al. 2008, *Nature*, 452, 851
- . 2016, *ApJ*, 819, L37
- van Haasteren, R., & Vallisneri, M. 2015, *MNRAS*, 446, 1170
- Vaughan, S., Uttley, P., Markowitz, A. G., et al. 2016, *MNRAS*, 461, 3145
- Verbiest, J. P. W., et al. 2016, *MNRAS*, 458, 1267
- Wang, J.-M., Songsheng, Y.-Y., Li, Y.-R., & Yu, Z. 2018, *ApJ*, 862, 171
- Xin, C., Charisi, M., Haiman, Z., et al. 2019, *arXiv e-prints*, arXiv:1907.11246
- Yan, C.-S., Lu, Y., Dai, X., & Yu, Q. 2015, *ApJ*, 809, 117
- Yu, Q. 2002, *MNRAS*, 331, 935
- Zheng, Z.-Y., Butler, N. R., Shen, Y., et al. 2016, *ApJ*, 827, 56
- Zhu, X.-J., Cui, W., & Thrane, E. 2019, *MNRAS*, 482, 2588
- Zhu, X.-J., et al. 2014, *MNRAS*, 444, 3709
- Zu, Y., Kochanek, C. S., Kozłowski, S., & Udalski, A. 2013, *ApJ*, 765, 106

APPENDIX

A. THE RED-NOISE MODEL

Here in Figure 4 we show the covariance function (left panel) and power spectral density (right panel) for the red-noise model considered in this work. Black dashed lines are for the damped random walk model, i.e., $\gamma = 1$, and coloured lines are for different values of γ . The grey vertical line on the right panel indicates $1/T_{\text{obs}}$ where $T_{\text{obs}} = 15.84$ yr is the data span of PG1302–102. The time scale τ_0 is set to be 1 yr in this example.

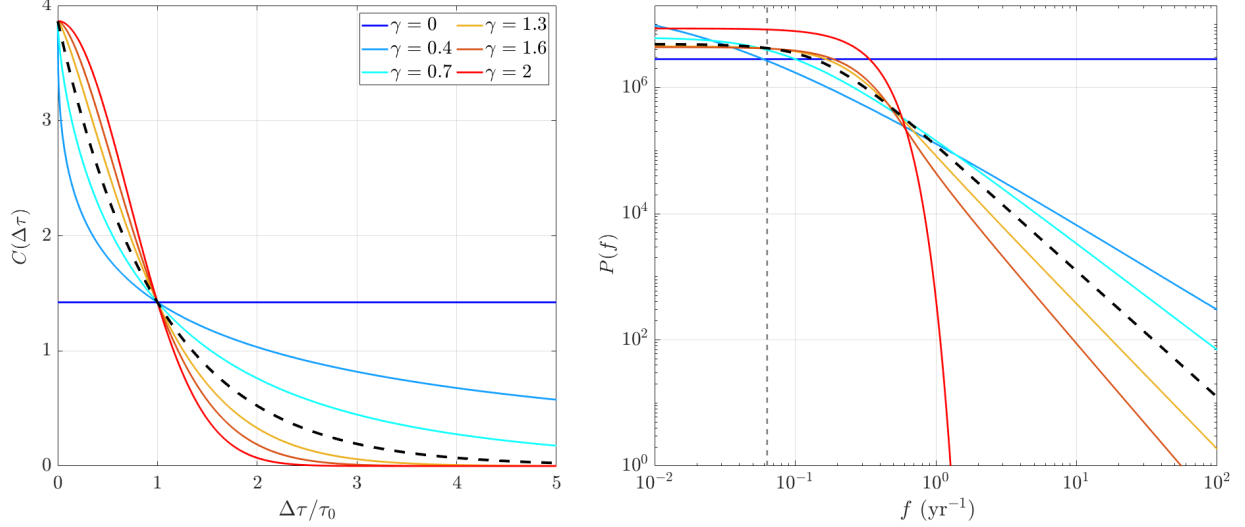


Figure 4. The covariance function $C(\Delta\tau)$ (left) and power spectral density $P(f)$ (right) for different values of γ (see Equation 6). Black dashed lines are given by $\gamma = 1$, i.e., the damped random walk model. The grey vertical line corresponds to the data span of $T_{\text{obs}} = 15.84$ yr for PG1302–102.

B. POSTERIOR DISTRIBUTIONS FROM ANALYSIS OF REAL DATA

Here we present full posterior distributions from the analysis of the combined data set (Figure 1) from CRTS, LINEAR and ASAS-SN for PG1302–102. Figure 5 shows the distributions for the red-noise hypothesis, whereas Figure 6 shows results for the sinusoidal signal plus red-noise hypothesis.

C. POSTERIOR DISTRIBUTIONS FROM ANALYSIS OF SIMULATED DATA

Here we present full posterior distributions from the analysis of a simulated data set (Figure 3) that includes an injected sinusoidal signal for PG1302–102. Figure 7 shows the distributions for original data, whereas Figure 8 shows results for the binned data with an interval of 100 days.

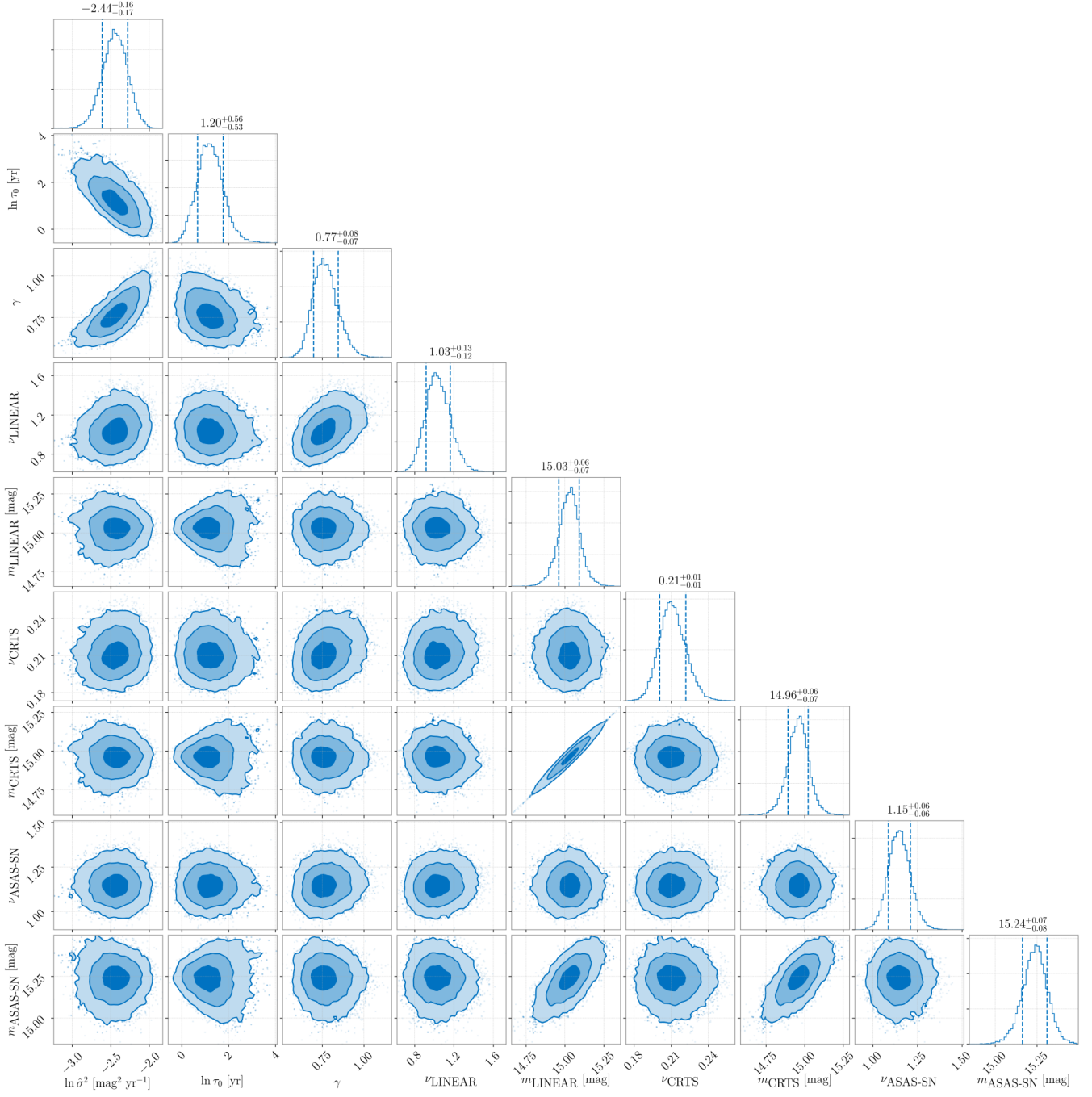


Figure 5. Posterior distributions of parameters for the red-noise hypothesis for the light curve of PG1302-102.

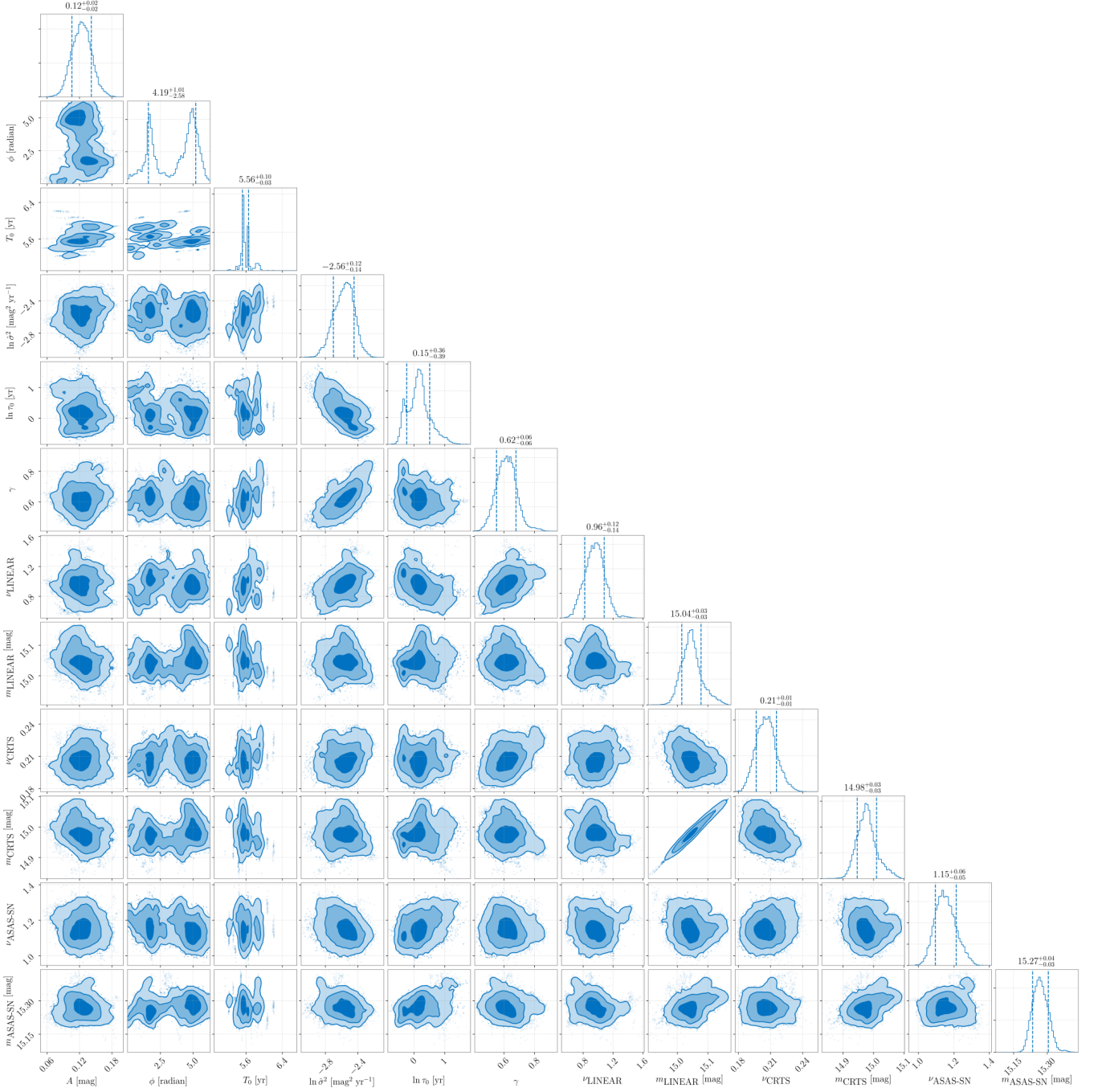


Figure 6. Posterior distributions of parameters for hypothesis that the light curve of PG1302-102 is modeled as a periodic signal in the presence of a red noise process.

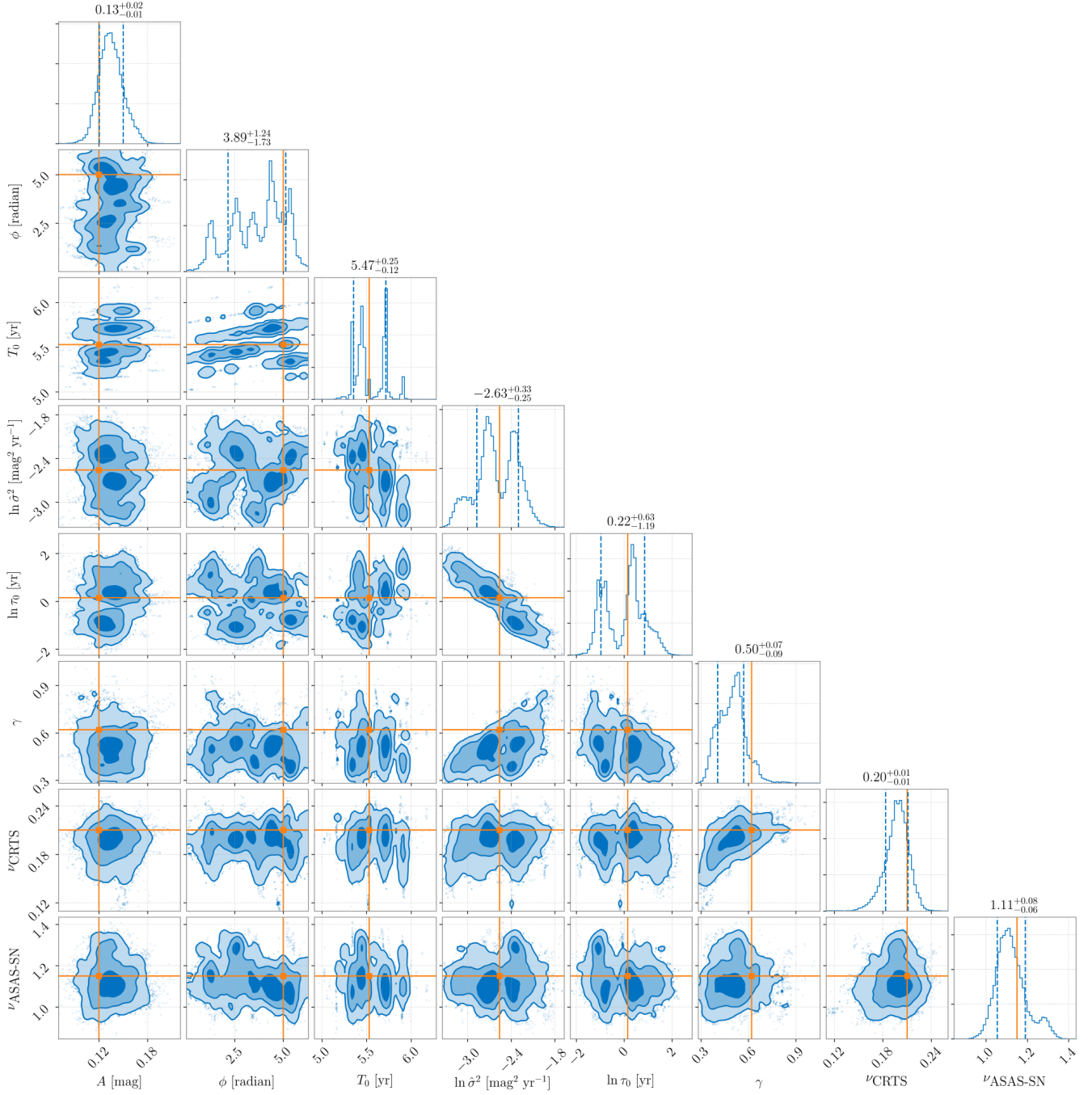


Figure 7. Posterior distributions of parameters for the sinusoidal signal plus red noise hypothesis for a simulated data set of PG1302–102 (shown in Figure 3), which included an injected signal. Orange lines mark the injection values.

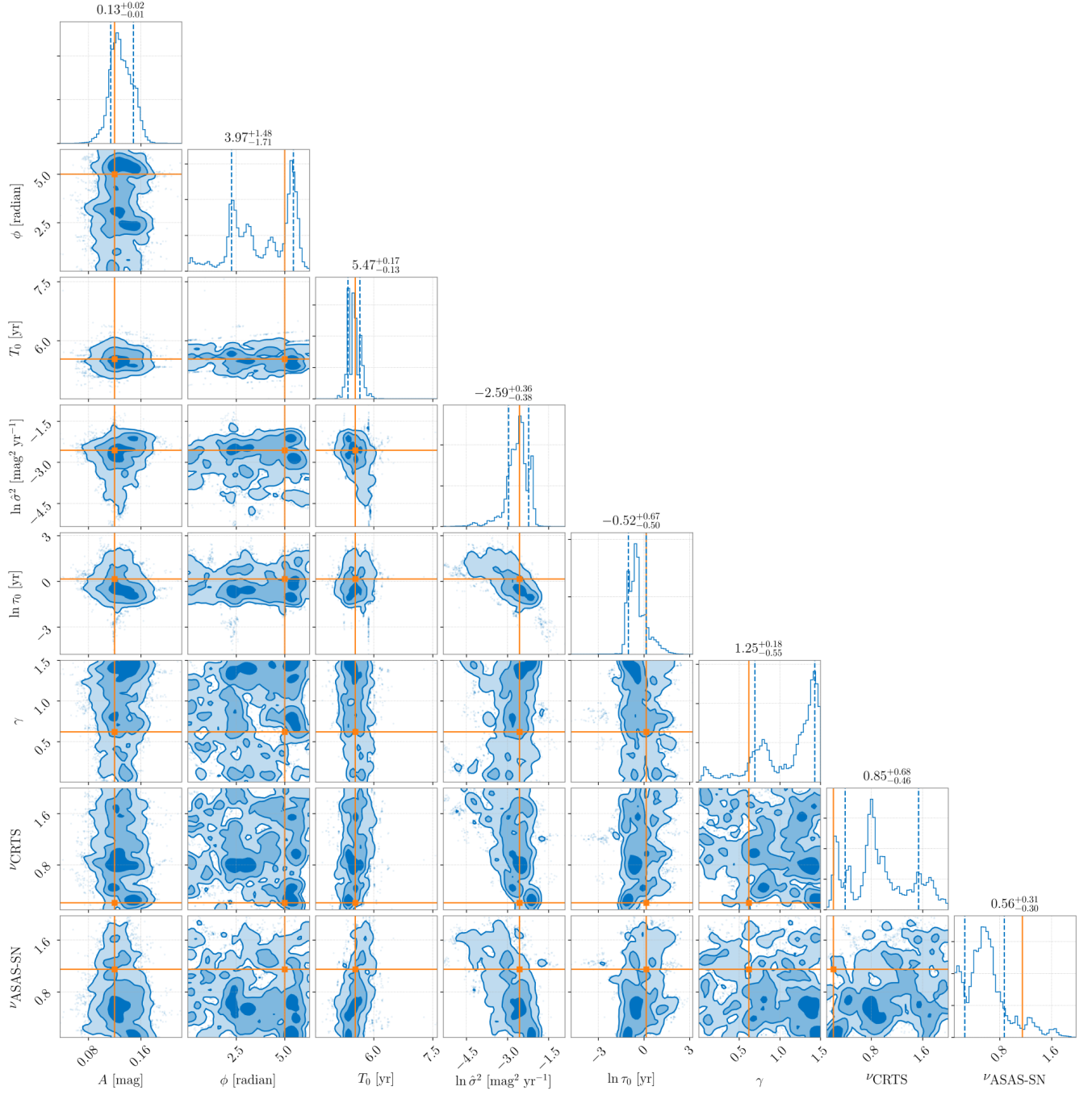


Figure 8. Same as Figure 7 but for the binned data with an interval of 100 days.